

Simulation of cardiac pathologies using an electromechanical biventricular model and XMR interventional imaging

M. Sermesant^a, K. Rhode^a, G.I. Sanchez-Ortiz^b, O. Camara^a,
R. Andriantsimiavona^a, S. Hegde^a, D. Rueckert^b, P. Lambiase^c, C. Bucknall^c,
E. Rosenthal^c, H. Delingette^d, D.L.G. Hill^{a,*}, N. Ayache^d, R. Razavi^a

^a Cardiac MR Research Group, King's College London, 5th Floor Thomas Guy House, Guy's Hospital, London, UK

^b Department of Computing, Imperial College London, UK

^c Department of Cardiology, St. Thomas' Hospital, London, UK

^d Epidaure Project, INRIA, Sophia Antipolis, France

Available online 11 July 2005

Abstract

Simulating cardiac electromechanical activity is of great interest for a better understanding of pathologies and for therapy planning. Design and validation of such models is difficult due to the lack of clinical data. XMR systems are a new type of interventional facility in which patients can be rapidly transferred between X-ray and MR systems. Our goal is to design and validate an electromechanical model of the myocardium using XMR imaging. The proposed model is computationally fast and uses clinically observable parameters. We present the integration of anatomy, electrophysiology, and motion from patient data. Pathologies are introduced in the model and simulations are compared to measured data. Initial qualitative comparison on the two clinical cases presented is encouraging. Once fully validated, these models will make it possible to simulate different interventional strategies.
© 2005 Elsevier B.V. All rights reserved.

Keywords: Data fusion; Patient-specific model; Electrophysiology study; Electromechanical coupling; Interventional imaging; Cardiac pathologies

1. Introduction

Simulation of the electromechanical activity in the heart is a very active research area. Recent progress in the understanding of cardiac function, and developments in modelling capabilities have made an integrative model of the heart conceivable (Hunter et al., 1997; McCulloch et al., 1998; Ayache et al., 2001; Geerts et al., 2003). However, building these models from in vivo human data is extremely difficult: most of the data

used comes from animal models or ex vivo data (frequently ex vivo animal models). The greatest clinical interest in modelling the heart, however, is in simulations of cardiovascular pathologies, and in customising the model to individual patients. To our knowledge, no electromechanical models of the heart have previously been built using in vivo human data from subjects with pathology, from which integrated anatomical, motion and electrical measurements are available.

This paper presents the integration of a previously described electromechanical model of the heart with clinical data from patients with heart rhythm abnormalities. Our approach is designed such that (i) the parameters of the model can be rapidly adjusted to a particular patient and (ii) direct comparisons can be made of the

* Corresponding author.

E-mail addresses: maxime.sermesant@kcl.ac.uk (M. Sermesant), derek.hill@ieee.org (D.L.G. Hill).

model and clinical measurements. An overview of the proposed methodology is presented in Fig. 1.

In Guy's Hospital, London, we have a catheterisation lab which incorporates both MRI and conventional fluoroscopy (XMR suite). XMR systems are a new type of interventional facility in which patients can be rapidly transferred between X-ray and MR systems on a floating table. The use of both modalities during interventions enables almost simultaneous collection of accurate cardiac anatomy, myocardial motion and electrical activity of the heart.

We have previously developed an XMR registration technique between MR and X-ray images obtained from such systems using real-time optical device tracking and projection calibration (Rhode et al., 2003, 2005). The registered data sets are used to initialise the model, which then simulates the assessed pathology. Thereafter, the computed behaviour is analysed and some of the pathological parameters can be used to test the consistency of the model.

Such an approach allows multiple validations, by testing a variety of patient-specific models against in vivo clinical data. Furthermore, these validations will guide the model design and future improvements. The various pathologies assessed during interventions will determine which parameters have to be included in the model, and how they need to be modified in order to reproduce abnormal cardiac function. It is crucial to ensure that the chosen model is not only able to reproduce the observed pathological behaviour but also able to provide predictive insights on the intervention procedure. The introduction of models in a clinical XMR setup opens up possibilities to compare the behaviour of the model with patient data before and after intervention. Our future work includes testing the predictive value of the model by simulating the intervention procedure and comparing the resulting cardiac function with the post-interventional data.

We are currently carrying out a clinical programme of XMR guided cardiac electrophysiology study (EPS) and radio-frequency ablation (RFA). The long term

aim of this work is to devise less invasive electrophysiology studies for the correction of abnormal heart rhythms and to assist in interventions. One part of this work is to estimate location of abnormal regions where ablation might be required from MRI (Sanchez-Ortiz et al., 2004b), and to compare pre- and post-intervention images MR images (Sanchez-Ortiz et al., 2004a). We present here our work on simulating the pathologies in order to better understand the electromechanical coupling and plan interventions.

The first part of this paper introduces the developed anatomical model and the electromechanical equations used to simulate cardiac function. Then, we present the integration of the different interventional clinical data into a common space. Finally, we describe the initialisation of the model from interventional data and the simulation of cardiac pathologies for two clinical cases.

2. Generic anatomical heart model

Simulation of the cardiac electromechanical activity requires myocardium geometry and muscle fibre orientations, which are important for both the active and passive behaviour of the myocardium, as well as for action potential propagation. It is difficult to obtain simultaneously both types of information for a particular myocardium. Geometry can be extracted from medical images, but diffusion tensor MRI (Hsu and Henriquez, 2001) cannot yet be applied to measure fibre orientation in vivo. When fibre orientations are measured from dissection (Guccione and McCulloch, 1991), the geometry is often not available, or is in such a deformed shape that adjustment of the model to the in vivo images becomes very challenging. To overcome these problems, we generate a synthetic model of the myocardium that we match to patient data.

2.1. 3D anatomical model image generation

2.1.1. Heart geometry

The left ventricle (LV) can be approximated with a truncated ellipsoid, as demonstrated by the classical use of this shape for LV volume estimation from 2D images (Mercier et al., 1982). The right ventricle (RV) can also be represented with a truncated ellipsoid. The generic heart model geometry is defined by: (1) the radii of both ellipsoids, (2) their thickness and (3) the height of the truncating basal plane (see Fig. 2).

2.1.2. Heart fibre orientations

Muscle fibre orientations change across the myocardial wall. In the heart model, the elevation angle between the fibre and the short axis plane varies between $+90^\circ$ and -90° from the endocardium to the epicardium (see Fig. 3). This is in good agreement with data avail-

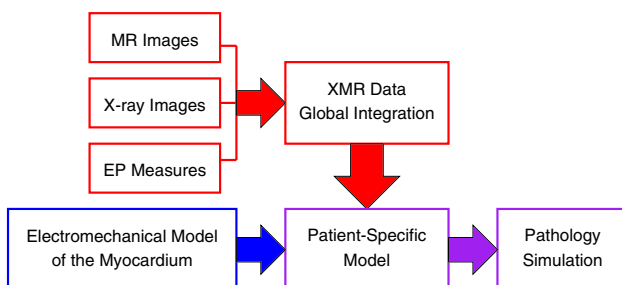


Fig. 1. Scheme of the method: XMR data integration is performed in order to adjust and initialise an electromechanical model of the myocardium, then the pathology is simulated with this patient-specific model.



Fig. 2. Generic anatomical heart model: short axis and long axis slices of geometry.

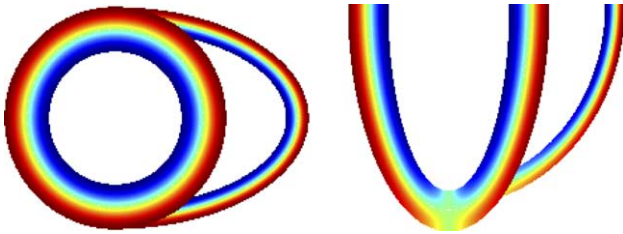


Fig. 3. Short axis and long axis slices of the synthetic fibre orientation. Colour: elevation angle with the short axis plane.

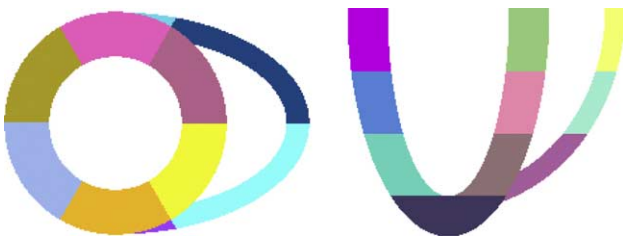


Fig. 4. Generic anatomical heart model: short axis and long axis slices of the anatomical segments defined by the AHA.

able in the literature from dissection or diffusion tensor MR (Hsu and Henriquez, 2001).

2.1.3. Cardiac anatomical divisions

We divide the synthetic model into the 17 regions of interest proposed by the American Heart Association (AHA) (Cerqueira et al., 2002) to ease calibration, estimation and analysis of the model (see Fig. 4).

2.2. 3D anatomical mesh generation

A triangulated surface is created using the marching cubes algorithm (Lorenson and Cline, 1987), optimised using the software YAMS,¹ and finally a tetrahedral mesh is generated with the software GHS3D² (30,000 elements). Fibre orientations and subdivisions are mapped into the mesh using a rasterisation process (Sermesant et al., 2003b). The resulting mesh is shown in Fig. 5.

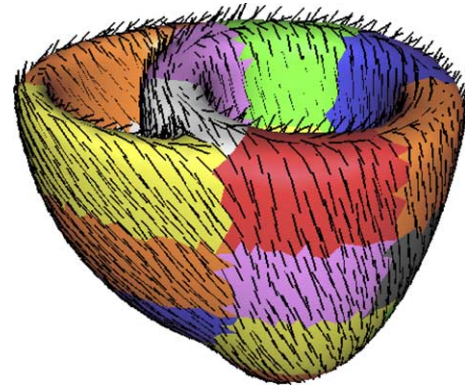


Fig. 5. Generic anatomical heart model: resulting mesh with fibre orientations (black segments) and AHA divisions (colours).

2.3. Model adjustment to patient anatomy

Automatic segmentation of the myocardium from MRI is still very challenging. We deform the generic anatomical model presented into the image. The proposed methodology is divided into three steps: segmentation of the image blood pools, registration for affine adjustment and deformable model for local fitting. First, the ventricular blood pools are segmented using a boundary- and region-based fuzzy classification method (Andriantsimiavona et al., 2003). Then, an automatic affine (including scaling and skew) registration algorithm is applied from the segmented image to the blood pools of the model. Finally, local adjustment is achieved using a deformable biomechanical model (Sermesant et al., 2003b), using as initial estimation the affine transformation previously computed.

This hierarchical procedure allows precise adjustment of the generic anatomical model to the patient image (Fig. 6). Biomechanical control for local deformation preserves surface smoothness and element numerical quality in contrast with other non-linear registration approaches.

3. Modelling the heart electromechanical activity

Understanding and modelling cardiac electrophysiology, studying the inverse problem from body surface potentials and direct measurement of heart potentials are active research areas (Katila et al., 2001; Magnin et al., 2003). Moreover, many constitutive laws have been proposed in the literature for the mechanical modelling of the myocardium (Hunter et al., 2003; Ayache, 2004).

All these models need rich local electromechanical data for validation. With animal models, macroscopic measurements of the electrical and mechanical activities of the same heart are now available (Faris et al., 2003). However, these data are difficult to obtain and very invasive.

¹ <http://www.ann.jussieu.fr/~frey/logiciels/yams.html>.

² <http://www-rocq.inria.fr/gamma/ghs3d/ghs.html>.

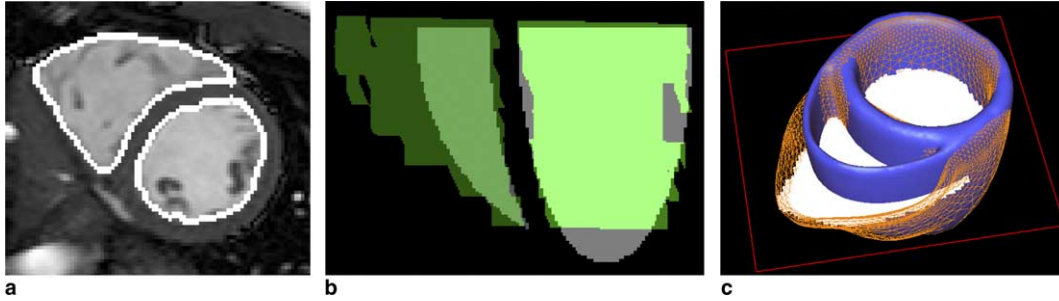


Fig. 6. Patient-specific model three steps: (a) semi-automatic segmentation of the blood pools (white contours), (b) affine registration between the model blood pools (grey) and the segmentation (green), (c) local adjustment (orange wire-frame) from the affine transform of the model (blue surface) using a deformable biomechanical model. (For interpretation of the references in colour in this figure legend, the reader is referred to the web version of this article.)

In the proposed approach, the validation of an electromechanical model of the human myocardium becomes possible, due to the integration of electrical and mechanical clinical data. Modelling choices are guided by both the nature of measurements (e.g., only extracellular potential is available for electrophysiology) and their resolution (e.g., spatial and temporal resolution of MR). This model helps to make the most of these measurements (extraction of hidden parameters, interpolation of sparse data), as well as to allow simulation of different pathologies and interventional strategies.

We proposed a simplified model of the cardiac electromechanical activity (Sermesant, 2003; Sermesant et al., 2004), which is used throughout this work. We only detail here the characteristics relevant for the presented clinical integration.

3.1. Simulation of the cardiac electrophysiology

Simulation of the cardiac electrophysiology is mostly done using either the *Luo-Rudy* or the *FitzHugh-Nagumo* types of models. The former is based on the simulation of all the different ions present in a cardiac cell along with the different channels. The latter type of model is based on a more global scale, only modelling electrical potential difference between the intracellular and the extracellular spaces (namely the action potential).

In a clinical context, it is possible to use invasive electrical recordings (Eldar et al., 1997; Schmitt et al., 1999; Okishige et al., 2003; Lambiase et al., 2004) to measure the isochrones of the depolarisation. The hidden parameter is therefore local conductivity, so we use a FitzHugh-Nagumo type of model. *Luo-Rudy* variables are not observable in vivo, and much too numerous to be adjusted from such data. We use the adapted version for cardiac cells of the FitzHugh-Nagumo equations proposed by Aliev and Panfilov (1996), in a simplified form:

$$\begin{cases} \partial_t u = \operatorname{div}(D\nabla u) + ku(1-u)(u-a) - uz, \\ \partial_t z = -\varepsilon(ku(u-a-1) + z), \end{cases}$$

where u is a normalised action potential, z is a secondary variable for the repolarisation, k and ε control the repolarisation, and a the reaction phenomenon. Parameter values are derived from Aliev and Panfilov (1996): $\varepsilon = 0.01$, $k = 8$, $a = 0.15$.

We introduce muscle fibre orientations in the computation through the diffusion tensor D , as they intervene in the propagation speed. This tensor represents the local conductivity. We solve these equations on the myocardium mesh built in the previous section using the finite element method. Further details about this electrical model can be found in (Sermesant et al., 2003a).

3.2. Simulation of the myocardium contraction

The action potential controls the mechanical contraction of the myocardium. In order to simulate this phenomenon, the constitutive law for the myocardium must include an active element, responding to an action potential by developing a contraction stress. We proposed a model (Sermesant, 2003; Sermesant et al., 2004), derived from a multi-scale modelling of the myocardium detailed in (Bestel et al., 2001).

This model is a combination of a linear visco-elastic passive constitutive law (parallel element), and an active contractile element that creates the contraction stress tensor (σ_c) controlled by the action potential

$$\partial_t \sigma_c = \sigma_0 |u|_+ - |u| \sigma_c,$$

where σ_0 is the maximum contraction, and $|u|_+$ the positive value of u .

This simplified constitutive law is represented by a damping matrix C for the internal viscosity part, a stiffness matrix K for the transverse anisotropic elastic part (parallel element) and a force vector F_c computed from the contraction stress tensor (contractile element). It can be integrated into the dynamics equation:

$$M \frac{d^2 U}{dt^2} + C \frac{dU}{dt} + KU = F_c + F_e,$$

where U is the displacement vector and F_e the external load force vector.

This model makes it possible to simulate the cardiac cycle, using different boundary conditions depending on the current phase: filling, isovolumetric contraction, ejection, or isovolumetric relaxation. The transition from one phase to another is automatically controlled by the pressure and the flow in the simulated model. Simulations of the normal cardiac function using this electromechanical model give a good representation of global and local behaviour of the myocardium (Sermesant, 2003; Sermesant et al., 2004).

4. Integration of clinical electromechanical data using XMR interventional imaging

The XMR interventional suite at King's College London (Guy's Hospital Campus, Fig. 7), comprises an X-ray and RF shielded room, with positive pressure air handling for sterility. The room contains a 1.5 T cylindrical bore MR scanner (Philips Intera I/T) and a mobile cardiac X-ray set (Philips BV Pulsera). The patient can be easily moved between the two systems using a specially modified sliding MR table top that docks with and transfers patients to a specially modified X-ray table (Philips Angio Diagnost 5 Syncratilt table). The docking and transfer takes less than 60 s. We have previously described the use of this system for guiding interventions on patients with congenital heart disease (Razavi et al., 2003).



Fig. 7. XMR suite at Guy's Hospital, London. (Front) X-ray C-arm system. (Back) MR scanner.

Using this system, we have access to different types of information: anatomy from 3D MR volume images, motion from multi-slice tagged MR images, invasive electrophysiology with electrical mapping system, and position of the mapping system within the MR images using XMR registration. The combination of these data provide very rich material for modelling the myocardium. Before using these data for modelling purposes, we have to integrate all different information in the same time-space coordinate system (Fig. 8).

The goal is to integrate the different available data to present a “virtual” heartbeat for which we would have simultaneously anatomy and motion from MR and electrophysiology from EPS.

4.1. Integration into the same spatial coordinates

The physical space used for spatial integration of these different datasets is the MR scanner space. We can locate the different MR images in this space owing to the information present in the DICOM headers, and the XMR registration makes it possible to transform the electrodes from the X-ray system space into the MR scanner space.

Although it is possible to acquire MR and X-ray images of the same patient during a procedure, the XMR system has no inherent ability to register these images. We have previously described the validation of a novel XMR registration technique that is applicable to the sliding table XMR configuration (Rhode et al., 2003, 2005).

The XMR registration technique aligns the MRI and electrophysiology data to an accuracy of 4–10 mm. For each of the two patients presented in this study, the 3D locations of the catheters that were visible in the X-ray images were reconstructed using biplane X-ray views, the registration matrices and the epipolar constraint. Reconstructed catheter paths were displayed in the segmented MR cardiac anatomy.

There are residual errors primarily due to respiratory motion and errors in the surface location from the EP system. Methods used to correct for these errors are presented in the following sections corresponding to each of the detailed clinical cases.

The different MR images acquired were analysed using different tools. The anatomical MR were manually segmented by an expert to isolate the anatomy of interest using the Analyze software package (Mayo Clinic, Minnesota, USA).

Tagged MR sequences were analysed to compute myocardium motion from the images. This motion was extracted using a non-rigid registration approach (Chandrashekhara et al., 2004). This method matches similar patterns in successive images without any tag line extraction.

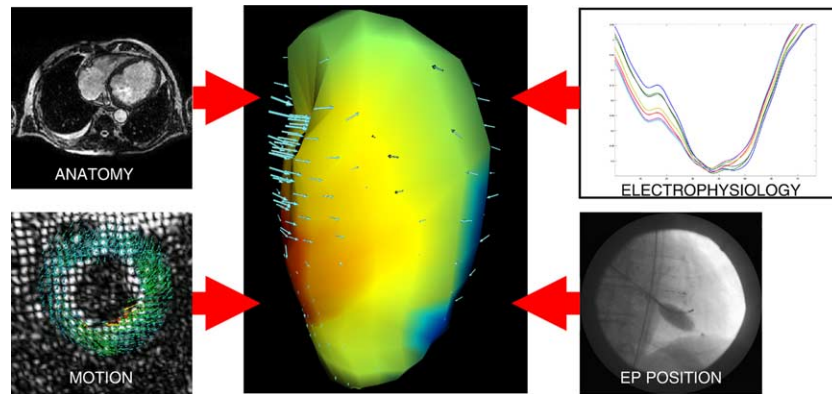


Fig. 8. Integration of the electromechanical data in the same time-space coordinate system.

4.2. Integration into the same time coordinates

To reconstruct this “virtual” heart beat, we also need to know the time correspondence between the different data sets. To achieve this, we need to know the heart rate and the instants of the measurements. For MR sequences, we can obtain this information from the headers of the data files (stored in DICOM format). Concerning the electrophysiology data, such information is also available in the recorded files.

In the case of intermittent pathologies, reconstructing this “virtual” heartbeat also depends on whether it was possible to image the patient in sustained arrhythmia or not.

We present in the following section how we performed the integration of the XMR data for two clinical cases, and how we simulated the two observed pathologies.

5. Clinical cases introduction

Cardiac arrhythmias are the cause of considerable morbidity and even occasional mortality (1.2 million hospitalisation and 480,000 deaths each year in the US, American Heart Association).³ Tachyarrhythmias (fast heart rhythms) can originate from ectopic foci of electrical depolarisation or from abnormal conduction pathways in the myocardium. The treatment of choice for patients with tachyarrhythmias is radio-frequency ablation (RFA), where the abnormal electrical focus or pathway is ablated by applying radio-frequency energy (Hebe et al., 2000). For patients with heart failure associated with ventricular asynchrony, the treatment of choice is biventricular pacing.

We present two clinical cases of cardiac arrhythmias. An electrophysiology study (EPS) is performed prior to

the interventions: an electrical measurement catheter is inserted into the appropriate chamber of the heart and the electrical activity on the endocardial surface is measured. For RFA procedures, the site of the abnormal focus or pathway can be determined from this electrical map (clinical case 2, Section 7). For biventricular pacing procedures, the optimal location of the pacing wires and the optimal pacing strategy can be determined (clinical case 1, Section 6).

There are several commercial systems available for carrying out EPS. They can be divided into two categories: contact and non-contact mapping systems. The former employs direct contact between measurement electrodes and the endocardium (clinical case 2, Section 7), whereas the latter uses extrapolation algorithms to extend electrical measurements made within the cardiac chambers to the endocardial surface (clinical case 1, Section 6).

6. Clinical case 1: left bundle branch block with scars

6.1. Case presentation

Patient 1, male, aged 68, had poor left ventricular function following a myocardial infarction. The patient was to undergo EPS and programmed pacing to assess the optimal location of pacing wires for biventricular pacing. The patient underwent sedation and local anaesthesia. Initially, MR imaging was performed. The cardiac anatomy was acquired using an SSFP three-dimensional multiphase sequence (3 phases, 256×256 matrix, 120 slices, resolution = $1.48 \times 1.48 \times 1.0$ mm³, TR = 3.2 ms, TE = 1.6 ms, flip angle = 45°). Myocardial motion imaging was performed in both short axis and long axis views using a CSPAMM spiral tagged imaging sequence (35 phases, 256×256 matrix, 9 slices SA & 5 slices LA, resolution = $1.76 \times 1.76 \times 12.0$ mm³, TR = 13.0 ms, TE = 1.1 ms, flip angle = 30°, tag spacing = 6 mm). The patient was then transferred to the

³ <http://www.americanheart.org>.

X-ray system. Three electrical measurement catheters were inserted into the patient's heart: a quadrapole catheter was placed in the right ventricle, the EnSite system's balloon catheter was placed in the left ventricle, and a decapole catheter, that acted as the EnSite system's roving catheter, was placed in the left ventricle. Initially, the roving catheter was moved along the endocardial surface of the left ventricle and the EnSite system tracked its position to generate a surface representation of this chamber. The electrical activity was then measured by the balloon catheter and mapped on the reconstructed left ventricular surface. Dynamic biplane tracked X-ray images were acquired with the catheters in place. Furthermore, locations of the 4 most distal electrodes on the roving catheter in the EnSite coordinate system were recorded. The X-ray imaging was carried out using end expiration breath holding to match the phase of respiration in which the MR images were acquired. The patient then underwent programmed pacing. The following day, late enhancement MR images were acquired to locate the myocardium scars, as part of this study. The patient had a successful pace-maker implantation at a later date.

6.2. XMR interventional measurements integration

6.2.1. Non-contact mapping system

Endocardial Solutions (ESI)⁴ supplies the EnSite non-contact electrical mapping system. It employs a catheter containing a flexible balloon made from a wire mesh (Fig. 9). The balloon is initially folded into the catheter bore and expands on deployment. It floats inside the desired cardiac chamber and does not contact the endocardial surface. The wire mesh intersection points on the balloon serve as electrodes and measure the electrical activity within the chamber. A second catheter, known as the roving catheter, is also inserted into the chamber. This catheter emits a radio-frequency signal from its tip that is detected by multiple sensors on the balloon. The location of the tip relative to the balloon is calculated using triangulation. The roving catheter is used to map the endocardial surface of the chamber by moving the catheter over this surface. The electrical activity measured by the balloon is then extrapolated to this surface and displayed by colour coding a surface rendering. The location of the roving catheter tip on the reconstructed endocardial surface is visualised and this catheter can be used to deliver either radio-frequency energy for ablation or pacing signals. Applications of this type of mapping system can be found in (Okishige et al., 2003; Lambiase et al., 2004).



Fig. 9. Catheter from endocardial solutions.

6.2.2. Non-rigid registration

The EnSite system estimates a surface of the left ventricle with the roving catheter, considering the furthest position as end-diastolic. When registered to the segmented MR anatomy with the XMR registration technology, some discrepancies between the two shapes appear. It is due to some residual errors in the XMR registration procedure and in the left ventricle endocardium estimation from the ESI system, which is difficult in the beating heart.

We correct this using a deformable surface technique (Montagnat and Delingette, 2001). A surface evolves under the influence of an external energy in order to adjust the surface to the image boundaries, computed from the gradient of the image, and an internal energy aiming at preserving the surface smoothness, computed from the curvature of the surface (Desbrun et al., 1999). For each vertex of the surface, a force proportional to the distance to the closest boundary point is applied along the normal of the surface. This method makes it possible to adjust the surface from the ESI system to the anatomy from MR, while ensuring a smooth surface (Fig. 10).

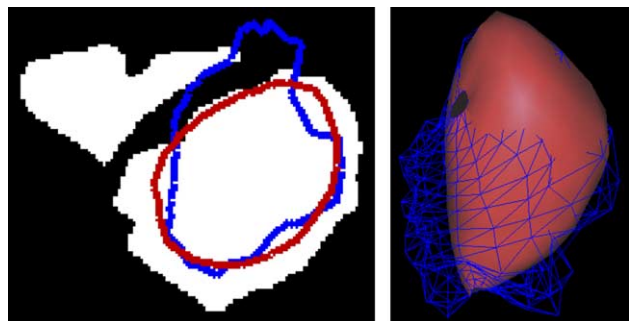


Fig. 10. Final registration between electrophysiology measurements and anatomy from MRI. Non-rigid registration of EnSite surface with segmented MR. Visualisation of initial (blue) and final (red) position and intersection with segmented MR (white). The orientation of the segmented slice is the same as in Fig. 12(a). (For interpretation of the references in colour in this figure legend, the reader is referred to the web version of this article.)

⁴ <http://www.endocardial.com>.

6.2.3. Global integration

Anatomy and motion from MR can be located in the same coordinates within the scanner space using information stored in DICOM headers. The integration of these different datasets makes it possible to visualise them in the same spatio-temporal coordinates (Fig. 11).

This integration makes it possible to visualise the electrophysiology propagation in the context of the patient anatomy. In this case, we can see the propagation coming from the septum, thus confirming the branch block. Moreover, this integration allows to see at the same time motion and electrophysiology, which is important to better understand and model the electromechanical coupling.

6.3. Pathology simulation: left bundle branch block with scars

6.3.1. Adjustment of the anatomical model to the patient anatomy

We adjust the generic anatomical model of the myocardium to the anatomical MR of the patient using the method described in Section 2.3. The semi-automatic segmentation of the blood pools is more challenging in the case of clinical axial images due to the intensity inhomogeneities in such big volumes and the absence of prior

knowledge on their geometry and topology in these coordinates, compared to the short axis ones. This is the reason why we can also observe in the segmentation a part of the atria. Nevertheless, satisfactory results were obtained, and the subsequent affine registration and local deformation provided a good adjustment of the model to this patient data (Fig. 12).

6.3.2. Initialisation of the electromechanical model from the integrated XMR measurements

The myocardium of this patient has scars from infarcted areas. Some of them can be observed in the late enhancement MR images. These scars led to a left bundle branch block (LBBB), which is observable in the electrophysiological measurements: the excitation in the left ventricle only comes from the septum area, without any other Purkinje excitation.

The scars were manually segmented by a clinical expert in the late enhancement images. Concerning the registration between the anatomical and the lesion images, we assumed that a linear transformation will cope with most significant differences between these acquisitions. Due to the short time passed between them, main differences are mostly caused by different breathing positions. As a matter of fact, a non-linear deformation could introduce some undesirable artifacts

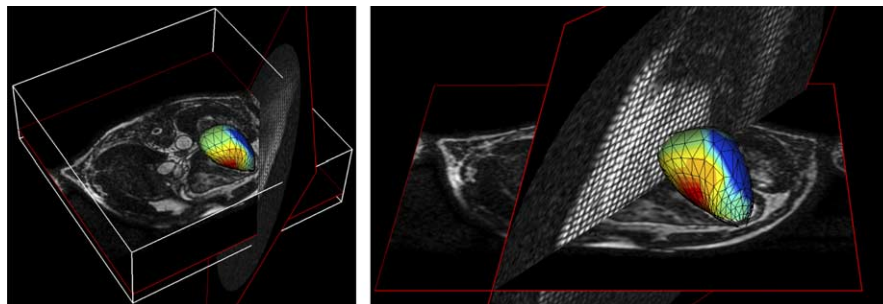


Fig. 11. Integration of electrophysiology, anatomy and motion in the same coordinates space, antero-lateral (left) and anterior (right) views (with different tagged MR slices). The measured isochrones are colour-coded on the deformed ESI surface.

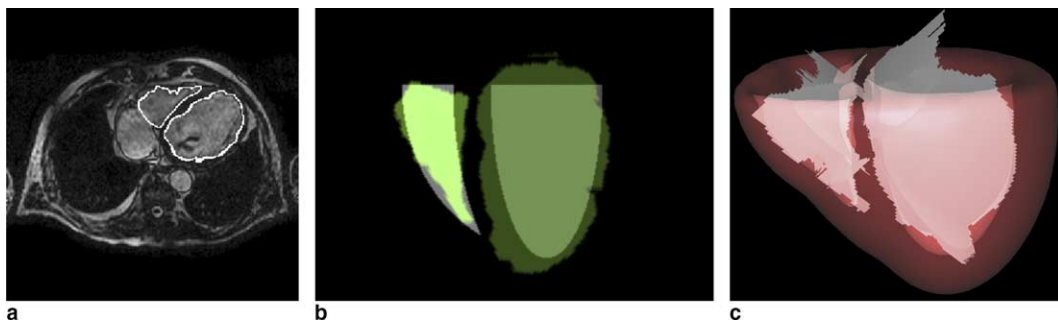


Fig. 12. Patient-specific anatomy of the model: (a) semi-automatic segmentation of axial MR blood pool, (b) affine registration between the model blood pools (grey) and the segmentation (green), (c) local adjustment of the deformable biomechanical model (red transparent surface) with the segmented image (white slices). (For interpretation of the references in colour in this figure legend, the reader is referred to the web version of this article.)

due to the similarity between the enhanced scars and the blood pool intensities.

Therefore, the affine registration procedure is computed between the grey-level late enhancement and anatomical MR images, using normalised mutual information as similarity measure. We obtain a good registration of the scars. Then we can integrate them in the model by a rasterisation process, assigning a different label to the tetrahedra containing some scar tissue (Fig. 13).

6.3.3. Simulation of the pathology

The branch block is simulated by removing the Purkinje network extremities in the left ventricle (Fig. 14). We simulate the effect of myocardial scars by modifying local conductivity and/or contractility parameters of the model in the corresponding tetrahedra. One goal of this work is to be able to estimate the electromechanical changes in the myocardium due to scars, using the model and the integrated data.

Moreover, this patient has an hypertrophied left ventricle (its end-diastolic volume segmented from MR is 400 mL whereas a normal left ventricle is around 130 mL). The filling from normal atrial pressure of such a big heart is not important enough to ensure a good cardiac output. This is well represented by the model,

which shows poor ejection with normal atrial pressure. In this kind of pathology, the heart adapts by increasing the end-diastolic pressure to allow a better filling of the ventricle. By integrating this into the model, using a pressure of 20 mmHg rather than 15 mmHg, we observe a better ejection.

Due to the left bundle branch introduction, the model reproduces a QRS complex of 180 ms, which is in agreement with the measured ECGs. This branch block also creates a desynchronisation between the phases of the two ventricles.

The simulated isochrones visually compare well with the measured ones, with the propagation on the left endocardium going from the septum to the free-wall. Quantitative comparison and adjustment is underway. The simulated ECG (precordial lead, simulated with an infinite conductivity thorax (Berenfeld and Jalife, 1998)) shows the characteristics of a left branch block, with a larger “M” shaped QRS complex. The lead is positioned using a mesh of the thorax manually registered with the MR image.

Moreover, the contraction is less efficient, and the left ventricle ejection starts later due to its late depolarisation, as can be seen in Fig. 15. The introduction of the scars in the model can change the electrical conductivity, the active mechanical properties, and the passive

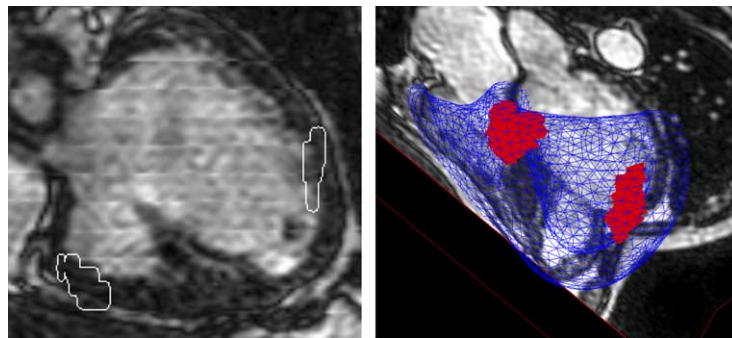


Fig. 13. (Left) Segmented scars registered into the anatomical MR, (right) scars integrated into the model through rasterisation of the scar image (red areas), presented within the anatomical image. (For interpretation of the references in colour in this figure legend, the reader is referred to the web version of this article.)

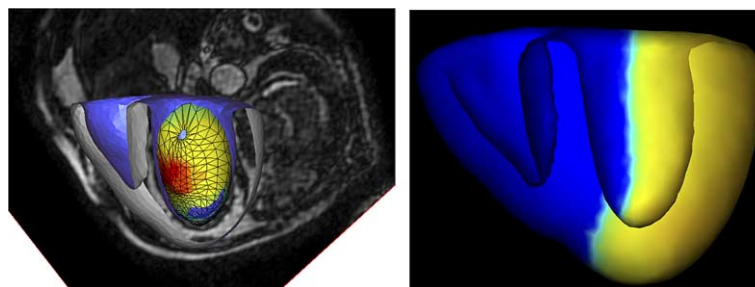


Fig. 14. Simulation of a left bundle branch block and scar effects. (Left) Model surface (blue), adjusted to patient anatomy (MR image) and isochrones from ESI system (coloured wire-frame). (Right) Simulated end-systolic position, with repolarisation wave coming from the right ventricle, due to the LBBB. (For interpretation of the references in colour in this figure legend, the reader is referred to the web version of this article.)

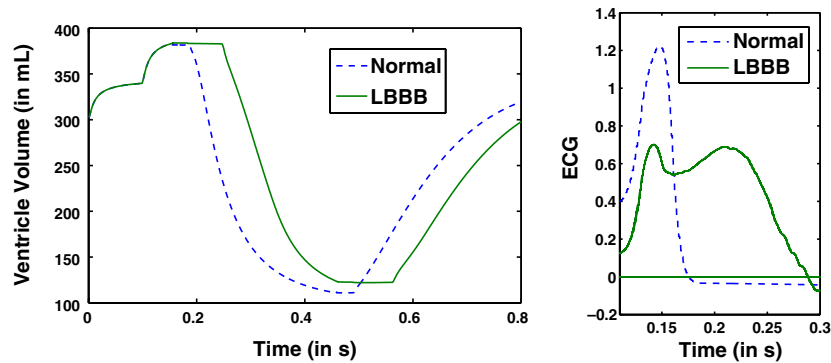


Fig. 15. (Left) Simulated left ventricle volume for patient anatomy heart (dashed) and with a left branch block and a scar (solid). (Right) Simulated ECGs: normal (dashed) and LBBB (solid).

mechanical properties. The integrated data make it possible to test different scars properties, and compare the simulated results with the patient data. The current cardiac function is still good compared to the one observed on the patient. Echocardiography assessed an ejection fraction of 20%. Myocardial contractility can still be quite efficient for scars involving less than 50% of myocardial thickness. In the current simulations, the scars represent less than 10% of the total mesh. Only the clearly enhanced scars have been integrated by now, but other parts in the late enhancement image have been identified as possible scars. The simulations could allow to test this hypothesis by comparing with the available motion data. It could help determine whether some hypersignals in these images do correspond to scars or not.

7. Clinical case 2: ventricular tachycardia

7.1. Case presentation

Patient 2, male, aged 15, had an intermittent ventricular tachycardia that was to be treated by EPS and RFA. The patient underwent paralysis and general anaesthesia prior to the procedure. Initially, MR imaging was performed. The cardiac anatomy was acquired using an SSFP three-dimensional multiphase sequence (5 phases, 256×256 matrix, 152 slices, resolution = $1.33 \times 1.33 \times 1.4 \text{ mm}^3$, TR = 3.0 ms, TE = 1.4 ms, flip angle = 45°). Myocardial motion imaging was performed in both short axis (SA) and long axis (LA) views using a SPAMM tagged imaging sequence (59 phase SA & 50 phases LA, 256×256 matrix, 11 slices SA & 4 slices LA, resolution = $1.33 \times 1.33 \times 8.0 \text{ mm}^3$, TR = 11.0 ms, TE = 3.5 ms, flip angle = 13° , tag spacing = 8 mm). The patient was then transferred to the X-ray system. Four electrical measurement catheters were inserted into the patient's right ventricle. Three of these were multipolar catheters and the fourth was a Constellation basket catheter. Dynamic biplane tracked X-ray images were acquired with the catheters in place and

the electrical activity was recorded at the same time from the Constellation catheter, in sinus rhythm and during ventricular ectopy. The X-ray image acquisition was carried out using ventilator control at end expiration to match the phase of ventilation during which the MR images were acquired. Unfortunately, it was not possible to reproduce sustained ventricular tachycardia in this patient during the EP study. The patient then underwent RFA.

7.2. XMR interventional measurements integration

7.2.1. Contact mapping system

The contact mapping system, supplied by Boston Scientific,⁵ employs the Constellation catheter, which is a multi-electrode basket catheter (Fig. 16). The basket consists of 8 splines with 8 electrodes on each, making a total of 64 electrodes. The splines are flexible and the basket is initially folded into the catheter bore, expanding when deployed from the tip of the catheter. The splines adapt to the endocardial surface and deform so that contact is maintained as the cardiac chamber contracts through the cardiac cycle. Electrical measurements can then be obtained for the myocardium region which is in contact with the electrodes. The electrograms are displayed as a series of graphical traces (Fig. 16). Applications of this type of mapping system can be found in (Eldar et al., 1997; Schmitt et al., 1999).

7.2.2. Rigid registration

We correct for residual mis-registration with a surface to image registration technique (Montagnat and Delingette, 1998) based on the Iterative Closest Point algorithm (Besl and McKay, 1992). For each vertex of the basket mesh, we compute the corresponding boundary voxel in the anatomical MR image by looking along the normal for a boundary point, defined from gradient magnitude and direction. Then, from all the matched

⁵ <http://www.bostonscientific.com>.

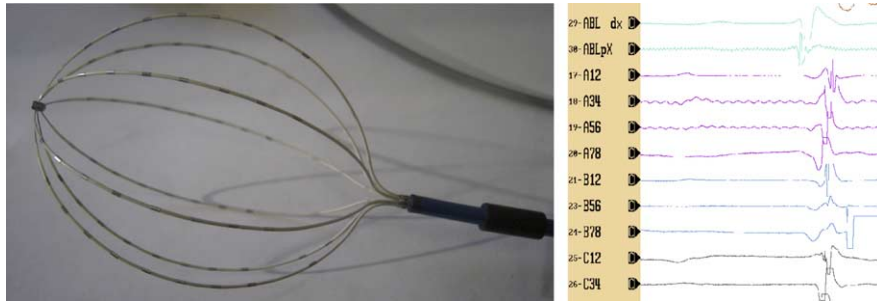


Fig. 16. The Constellation catheter from Boston Scientific, and some of the measured electrical potentials.

vertex/boundary point pairs, we estimate the best rigid body transformation, iterating until convergence.

This method allows to recover most of the residual error of the XMR registration procedure (Fig. 17). Local deformations could correct for the remaining difference, but this is not necessary for the use of the measures presented here.

7.2.3. Global integration

Anatomy and motion from MR can be located in the same coordinates within the scanner space using infor-

mation stored in DICOM headers. The integration of these different datasets makes it possible to visualise them in the same spatio-temporal coordinates (Fig. 18).

7.3. Pathology simulation: ectopic focus

7.3.1. Adjustment of the anatomical model to patient anatomy

We also adjust the generic anatomical model of the myocardium to the anatomical MR of the patient using the method described in Section 2.3. This method gives a

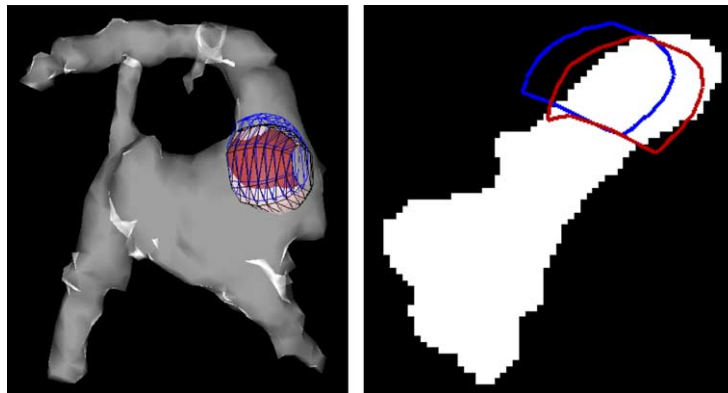


Fig. 17. Final registration between electrophysiology measurements and anatomy from MRI. Rigid registration of Constellation catheter surface with segmented MR. Visualisation of initial (blue) and final (red) position and intersection with segmented MR (white). (For interpretation of the references in colour in this figure legend, the reader is referred to the web version of this article.)

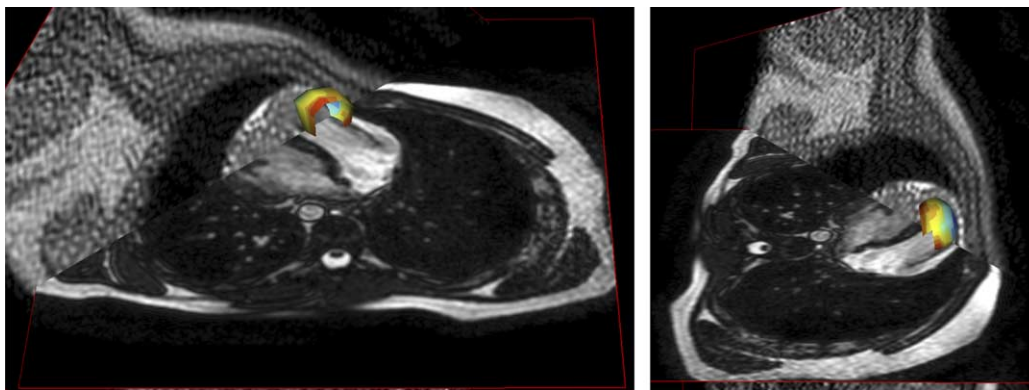


Fig. 18. Integration of electrophysiology (catheter), anatomy (MR) and motion (tagged MR) in the same coordinates space, posterior (left) and lateral (right) views. The measured isochrones are colour-coded on the Constellation catheter surface.

good agreement between the deformed mesh and the patient image (Fig. 19).

7.3.2. Initialisation of the electromechanical model from the integrated XMR measurements

An ectopic focus can be simulated by introducing an additional depolarising area in the model, located from the measured position with the Constellation catheter and the XMR registration procedure, and starting at the time given by the electrical recordings (Fig. 20).

The electromechanical model of the myocardium has been registered with the anatomical MR to obtain the patient geometry. Then, vertices corresponding to the ectopic focus are determined by looking for the closest vertices to the Constellation electrodes where this focus is observed.

The timing of the ectopic beat is deduced from observation of the electrical recordings, which also comprise several ECG derivations.

7.3.3. Simulation of the pathology

The ectopic focus being localised in the myocardium, an ectopic beat can be simulated. The ectopic excitation takes place during the P wave, before the normal QRS complex (see Fig. 21).

We can observe in the simulation results that the early contraction of the myocardium from the ectopic

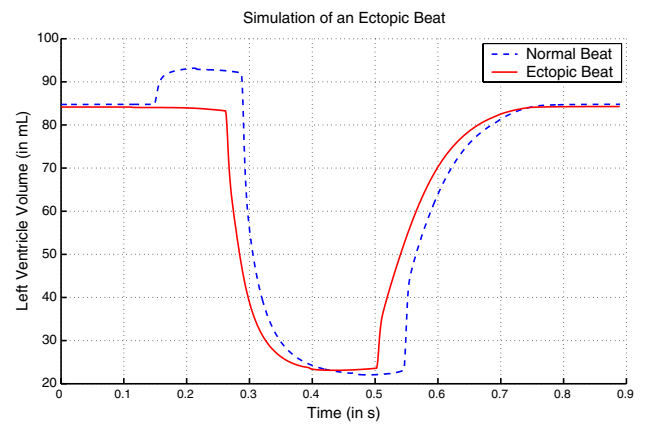


Fig. 21. Consequences on cardiac function parameters: comparison between the simulated normal (dashed) and the simulated ectopic (solid) left ventricle volume.

excitation prevents the atrial contraction from filling the ventricles completely. The ejected volume drops from 71 to 61 mL.

Moreover, the simulation of several ectopic beats leads to an even greater difference, with a smaller end-diastolic volume for the heart model in ectopic tachycardia. Thus, the consequences of this arrhythmia on the simulated cardiac function are well represented. As we could not induce sustained arrhythmia during the image

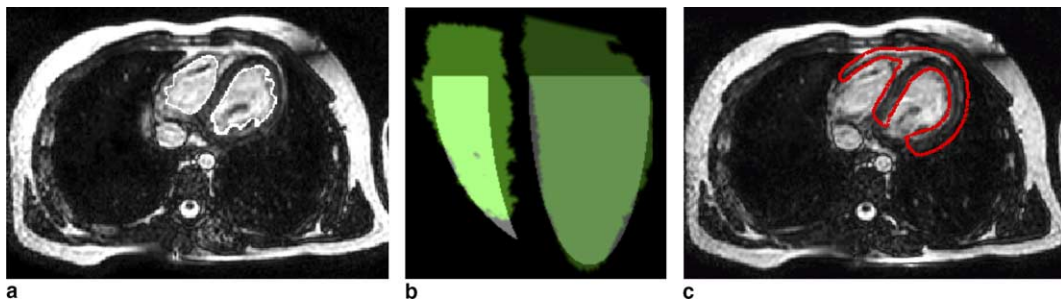


Fig. 19. Patient-specific anatomy of the model: (a) semi-automatic segmentation of axial MR blood pool, (b) affine registration between the model blood pools and the segmentation, (c) local adjustment of the deformable biomechanical model, intersection between the deformed model and the MR image.

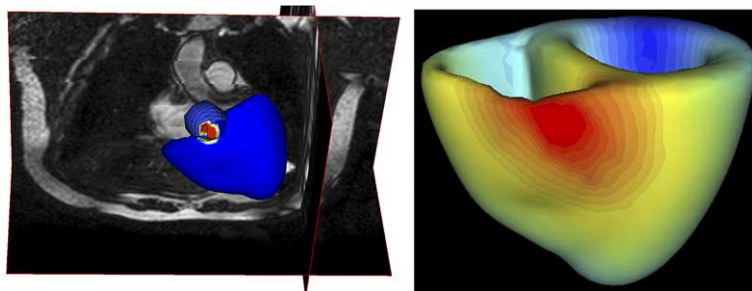


Fig. 20. Simulation of an ectopic focus from XMR measurements. (Left) Model adjusted to patient anatomy with MR, visualisation of Constellation catheter (meshed sphere), MR anatomy and bi-ventricular myocardium model. Colour: electrical potential when ectopic beat starts. (Right) Isochrones of the simulation of the ectopic beat (red to blue: 0 to 160 ms). (For interpretation of the references in colour in this figure legend, the reader is referred to the web version of this article.)

acquisition, we cannot adjust the pathological mechanical parameters of the patient from images. But current work on ECG simulation will make it possible to validate the electrical propagation with the measured ECGs.

8. Conclusion

In this paper, we have constructed electromechanical models of the heart from patients with heart rhythm abnormalities. To our knowledge, this is the first time that in vivo human data has been used in the construction of such a model. We have made use of patient data collected from an XMR facility, that provides spatially integrated invasive electrical mapping and MR imaging, while the patient is in a single facility.

To generate our models efficiently, we have devised a technique to adapt a generic anatomical model to the patient anatomy from MRI. Using the XMR system, we have collected registered information about cardiac anatomy, motion and electrical activity from two patients with heart rhythm abnormalities. We have used integrated clinical patient data to initialise the models, and then simulated the assessed pathology. Initial results show good agreement between simulated values and clinical measurements. More quantitative validation is underway. The electrical measurements from the EPS allow to adjust the local conductivity of the model, with a specially designed method (Moreau-Villéger et al., 2004). Moreover, the motion obtained from the analysis of tagged images makes it also possible to design a local adjustment of the mechanical properties. The validation process will lead to refinements of the model, and will also enable to precisely identify required information to initialise the model.

Our long term aim is to use the model to devise less invasive techniques for EPS that could transform the clinical applicability and effectiveness of these procedures. Some example applications are biventricular pacing for treatment of heart failure and radio-frequency ablation of ventricular tachycardia. These procedures can be highly effective with minimal side effects, but have variable success rates, are often very long, and can involve high X-ray radiation dose to both patient and staff. There is thus a need for substantial innovation in order to reliably achieve successful results in an acceptable time, with lower radiation dose and reduced risk of accidental damage to adjacent structures. For instance, in the case of biventricular pacing, these models could provide a way to optimise the pacing leads position by looking at the simulated cardiac functions for different locations. In some patients with re-entry, ventricular or supra-ventricular tachycardia where standard ablation is often difficult, it would be possible to test different ablation strategies and optimise the procedure.

Acknowledgements

The authors thank for their collaboration the Cardiac MR Research Group in Guy's Hospital, London and the co-workers of the ICEMA collaborative research actions^{6,7} funded by INRIA and coordinated by F. Clément and M. Sorine. The authors acknowledge grant support from EPSRC (M.S., K.R., G.S., O.C. and R.A.). The authors thank P. Moireau for thoughtful discussions.

References

- Aliev, R., Panfilov, A., 1996. A simple two-variable model of cardiac excitation. *Chaos, Solitons & Fractals* 7 (3), 293–301.
- Andriantsimivavona, R., Griffin, L., Hill, D., Razavi, R., 2003. Simple cardiac MRI segmentation. In: *International Society for Magnetic Resonance in Medicine Scientific Meeting*, vol. 6, p. 951.
- Ayache, N. (Ed.), 2004. *Computational Models for the Human Body*. Ciarlet, P. (Ed.). *Handbook of Numerical Analysis*. Elsevier, Amsterdam.
- Ayache, N., Chapelle, D., Clément, F., Coudière, Y., Delingette, H., Désidéri, J., Sermesant, M., Sorine, M., Urquiza, J., 2001. Towards model-based estimation of the cardiac electro-mechanical activity from ECG signals and ultrasound images. In: *Functional Imaging and Modeling of the Heart (FIMH'01)*. *Lecture Notes in Computer Science (LNCS)*, vol. 2230. Springer, Berlin, pp. 120–127.
- Berenfeld, O., Jalife, J., 1998. Purkinje-muscle reentry as a mechanism of polymorphic ventricular arrhythmias in a 3-dimensional model of the ventricles. *Circulation Research* 82 (10), 1063–1077.
- Besl, P., McKay, N., 1992. A method for registration of 3D shapes. *IEEE Transactions on Pattern Analysis and Machine Intelligence* 14 (2), 239–256.
- Bestel, J., Clément, F., Sorine, M., 2001. A biomechanical model of muscle contraction. In: *Medical Image Computing and Computer-Assisted Intervention (MICCAI'01)*. *Lecture Notes in Computer Science (LNCS)*, vol. 2208. Springer, Berlin, pp. 1159–1161.
- Cerqueira, M., Weissman, N., Dilsizian, V., Jacobs, A., Kaul, S., Laskey, W., Pennell, D., Rumberger, J., Ryan, T., Verani, M., 2002. Standardized myocardial segmentation and nomenclature for tomographic imaging of the heart. *Circulation* 105, 539–542.
- Chandrashekhara, R., Mohiaddin, R., Rueckert, D., 2004. Analysis of 3-D myocardial motion in tagged MR images using nonrigid image registration. *IEEE Transactions on Medical Imaging* 23 (10), 1245–1250.
- Desbrun, M., Meyer, M., Schröder, P., Barr, A., 1999. Implicit fairing of arbitrary meshes using diffusion and curvature flow. In: *International Conference on Computer Graphics and Interactive Techniques (ACM Siggraph'99)*. ACM Press/Addison-Wesley, New York/Reading, MA, pp. 317–324.
- Eldar, M., Ohad, D., Goldberger, J., Rotstein, Z., Hsu, S., Swanson, D., Greenspon, A., 1997. Transcutaneous multielectrode basket catheter for endocardial mapping and ablation of ventricular tachycardia in the pig. *Circulation* 96 (7), 2430–2437.
- Faris, O., Evans, F., Ennis, D., Helm, P., Taylor, J., Chesnick, A., Guttman, M., Ozturk, C., McVeigh, E., 2003. Novel technique for cardiac electromechanical mapping with magnetic resonance imaging tagging and an epicardial electrode sock. *Annals of Biomedical Engineering* 31 (4), 430–440.

⁶ <http://www-rocq.inria.fr/who/Frederique.Clement/icema.html>.

⁷ <http://www-rocq.inria.fr/sousso/icema2/icema2.html>.

- Geerts, L., Kerckhoffs, R., Bovendeerd, P., Arts, T., 2003. Towards patient specific models of cardiac mechanics: a sensitivity study. In: International Symposium on Surgery Simulation & Soft Tissue Modeling (IS4TM'03). Lecture Notes in Computer Science (LNCS), vol. 2230. Springer, Berlin, pp. 00–11.
- Guccione, J., McCulloch, A., 1991. Theory of heart: biomechanics, biophysics, and nonlinear dynamics of cardiac function. Finite Element Modeling of Ventricular Mechanics. Springer-Verlag, Berlin, pp. 121–144.
- Hebe, J., Hansen, P., Ouyang, F., Volkmer, M., Kuck, K., 2000. Radiofrequency catheter ablation of tachycardia in patients with congenital heart disease. *Pediatric Cardiology* 21 (6), 557–575.
- Hsu, E., Henriquez, C., 2001. Myocardial fiber orientation mapping using reduced encoding diffusion tensor imaging. *Journal of Cardiovascular Magnetic Resonance* 3, 325–333.
- Hunter, P., Nash, M., Sands, G., 1997. Computational biology of the heart Chapter 12. *Computational Electromechanics of the Heart*. Wiley, New York, pp. 345–407.
- Hunter, P., Pullan, A., Smaill, B., 2003. Modeling total heart function. *Annual Review of Biomedical Engineering* 5, 147–177.
- Katila, T., Magnin, I., Clarysse, P., Montagnat, J., Nenonen, J. (Eds.), 2001. *Functional Imaging and Modeling of the Heart (FIMH'01)*. Lecture Notes in Computer Science (LNCS), vol. 2230. Springer, Berlin.
- Lambiase, P., Rinaldi, A., Hauck, J., Mobb, M., Elliott, D., Mohammad, S., Gill, J., Bucknall, C., 2004. Non-contact left ventricular endocardial mapping in cardiac resynchronisation therapy. *Heart* 90 (1), 44–51.
- Lorensen, W., Cline, H., 1987. Marching cubes: a high resolution 3D surface reconstruction algorithm. *Computer Graphics (Proceedings of SIGGRAPH)* 21 (4), 163–169.
- Magnin, I., Montagnat, J., Clarysse, P., Nenonen, J., Katila, T. (Eds.), 2003. *Functional Imaging and Modeling of the Heart (FIMH'03)*. Lecture Notes in Computer Science (LNCS), vol. 2674. Springer, Berlin.
- McCulloch, A., Bassingthwaite, J., Hunter, P., Noble, D., Blundell, T., Pawson, T., 1998. Computational biology of the heart: from structure to function. *Progress in Biophysics & Molecular Biology* 69 (2/3), 151–559.
- Mercier, J., DiSessa, T., Jarmakani, J., Nakanishi, T., Hiraishi, S., Isabel-Jones, J., Friedman, W., 1982. Two-dimensional echocardiographic assessment of left ventricular volumes and ejection fraction in children. *Circulation* 65, 962–969.
- Montagnat, J., Delingette, H., 1998. Globally constrained deformable models for 3D object reconstruction. *Signal Processing* 71 (2), 173–186.
- Montagnat, J., Delingette, H., 2001. A review of deformable surfaces: topology, geometry and deformation. *Image and Vision Computing* 19 (14), 1023–1040.
- Moreau-Villéger, V., Delingette, H., Sermesant, M., Faris, O., McVeigh, E., Ayache, N., 2004. Global and local parameter estimation of a model of the electrical activity of the heart. Tech. rep., INRIA.
- Okishige, K., Kawabata, M., Umayahara, S., Yamashiro, K., Gotoh, M., Isobe, M., Strickberger, S., 2003. Radiofrequency catheter ablation of various kinds of arrhythmias guided by virtual electrograms using a noncontact, computerized mapping system. *Circulation Journal* 67 (5), 455–460.
- Razavi, R., Hill, D.L., Keevil, S., Miquel, M., Muthurangu, V., Hegde, S., Rhode, K., Barnett, M., van Vaals, J., Hawkes, D., Baker, E., 2003. Cardiac catheterisation guided by MRI in children and adults with congenital heart disease. *Lancet* 362 (9399), 1877–1882.
- Rhode, K., Hill, D., Edwards, P., Hipwell, J., Rueckert, D., Sanchez-Ortiz, G., Hegde, S., Rahunathan, V., Razavi, R., 2003. Registration and tracking to integrate X-ray and MR images in an XMR facility. *IEEE Transactions on Medical Imaging* 22 (11), 1369–1378.
- Rhode, K., Sermesant, M., Brogan, D., Hegde, S., Hipwell, J., Lambiase, P., Rosenthal, E., Bucknall, C., Qureshi, S., Gill, J., Razavi, R., Hill, D., 2005. A system for real-time XMR guided cardiovascular intervention. *IEEE Transactions on Medical Imaging* (accepted).
- Sanchez-Ortiz, G., Chandrashekar, R., Rhode, K., Razavi, R., Hill, D., Rueckert, D., 2004a. Detecting regional changes in myocardial contraction patterns using MRI. In: *SPIE Medical Imaging 2004*, 710–721.
- Sanchez-Ortiz, G., Sermesant, M., Chandrashekar, R., Rhode, K., Razavi, R., Hill, D., Rueckert, D., 2004b. Detecting the onset of myocardial contraction for establishing inverse electro-mechanical coupling in XMR guided RF ablation. In: *Proceedings of IEEE International Symposium on Biomedical Imaging*, Arlington, USA, pp. 1055–1058.
- Schmitt, C., Zrenner, B., Schneider, M., Karch, M., Ndrepepa, G., Deisenhofer, I., Weyerbrock, S., Schreieck, J., Schomig, A., 1999. Clinical experience with a novel multielectrode basket catheter in right atrial tachycardias. *Circulation* 99 (18), 2414–2422.
- Sermesant, M., 2003. *Modèle électromécanique du cœur pour l'analyse d'images et la simulation*. Ph.D. Thesis, Université de Nice-Sophia Antipolis.
- Sermesant, M., Faris, O., Evans, F., McVeigh, E., Coudière, Y., Delingette, H., Ayache, N., 2003a. Preliminary validation using in vivo measures of a macroscopic electrical model of the heart. In: *International Symposium on Surgery Simulation and Soft Tissue Modeling (IS4TM'03)*. Lecture Notes in Computer Science (LNCS), vol. 2230. Springer, Berlin, pp. 230–243.
- Sermesant, M., Forest, C., Pennec, X., Delingette, H., Ayache, N., 2003b. Deformable biomechanical models: application to 4D cardiac image analysis. *Medical Image Analysis* 7 (4), 475–488.
- Sermesant, M., Delingette, H., Ayache, N., 2004. An electromechanical model of the myocardium for cardiac image analysis and medical simulation. Tech. rep., INRIA, in revision.